Combustion, Explosion, and Shock Waves, Vol. 43, No. 6, pp. 732–740, 2007

Simulation of Shock Wave Impact Due to Explosion on a Flying Flexible Aircraft

E. Carrera,[1] V. Morello,[1] D. Valletti,[1] and F. Algostino[1]

UDC 523.593

Translated from *Fizika Goreniya i Vzryva*, Vol. 43, No. 6, pp. 121–130, November–December, 2007.
Original article submitted June 27, 2006; revision submitted April 24, 2007.

This paper describes the results obtained by a computational simulation of the impact of shock waves due to explosion on a flying flexible aircraft of commercial type. An explicit three-dimensional dynamic nonlinear coupled analysis has been conducted by means of the software MSC.Dytran. A Lagrangian mesh has been used for the structural parts, and a Eulerian domain is used for the surrounding fluid. The fluid-dynamic solver uses a Eulerian approach and employs a finite volume method to discretize the governing equations. Structural elements are discretized by the Finite Element Method. The impact of the related shock waves on a simple panel and a wing box has been considered. The vibration of an aircraft as a whole, caused by its flexibility, has been analyzed. The analysis has mainly shown that the conducted investigation can be used to evaluate the loads on the aircraft for various initial positions of the explosion as well as for various amounts of the explosive charge. The method could permit a better design of the aircraft with respect to explosion phenomena and simulation of aircraft accidents, aimed at understanding their causes.

Key words: aeronautics, computational simulation of the impact of shock waves on a flexible aircraft, fluid–structure interaction.

INTRODUCTION

The development of computational mechanics in the last two decades has permitted the simulation of explosion phenomena in various applications [1–6]. In the present paper, the attention is restricted to aeronautics: effect of the explosion on aircraft elements. To the best of the authors' knowledge there are no results available on the evaluation of loads produced by an explosion in air on a flying aircraft, as well as of their effects on deformable structures. Such an analysis could permit the following interesting tasks: to evaluate the loads on the aircraft for various initial positions of the explosions and for various amounts of the high explosive (HE) charge, to make a better design of the aircraft with respect to explosion phenomena, and to simulate aircraft accidents to understand their causes.

The present work evaluates the possibility of using a commercial software (MSC.Dytran [7]) to simulate the loading that an explosion induces on a flying flexible aircraft.

1. SOME THEORETICAL CONSIDERATION

An explosion of a chemical HE in air is known to form a blast wave propagating from the explosion center to the ambient medium [8]. The pressure-time history of a typical blast wave as observed at a location removed from the explosion center is shown in Fig. 1. Positive and negative phases of pressure are observed; the negative pressure is bounded at approximately 1 atm.

Three independent characteristics have to be specified to describe a blast wave: shock intensity, duration of the blast wave, and its impulse. Shock intensity is obtained from the scaling law. It depends on the explosion distance, TNT equivalent detonated, and the

[1]Politecnico di Torino, 10129 Torino, Italy; erasmo.carrera@polito.it.

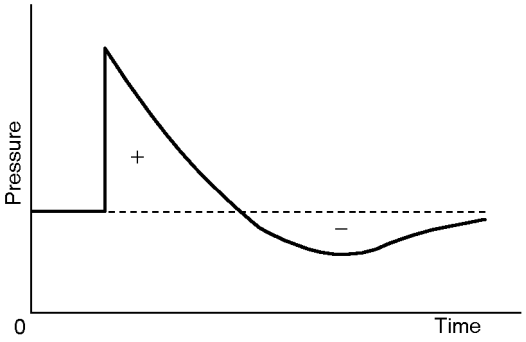

Fig. 1. Typical pressure–time curve for an explosion blast wave in air.

nature of the medium. The scaling law for explosion is based on fundamentals of geometrical similarity. Kinney and Graham derived the relation [8]

$$p^0/p_a = \frac{808\left[1+\left(\frac{Z}{4.5}\right)^2\right]}{\sqrt{1+\left(\frac{Z}{0.048}\right)^2}\sqrt{1+\left(\frac{Z}{0.32}\right)^2}\sqrt{1+\left(\frac{Z}{1.35}\right)^2}}, \tag{1}$$

where p^0 is the peak pressure, $Z = rf_d/W^{1/3}$ is the scaled distance, $f_d = (p_a/p_{0a})^{1/3}(T_{0a}/T_a)^{1/3}$ is a coefficient depending on ambient temperature and pressure and on their stagnation values, p_a and T_a are the ambient pressure and temperature, p_{0a} and T_{0a} are the ambient pressure and temperature at the sea level, respectively, r is the distance from the explosion point, and W is the equivalent TNT mass.

In addition to the peak pressure, the time duration of the blast wave is a fundamental parameter necessary to explore the wave ability to cause damage on the structures around. The positive pressure phase of the blast wave is the most damaging one; therefore, the duration of positive pressure can be taken as an index of the time duration for the entire blast wave system (even though, very often, the duration of the negative phase is at least twice the duration of the positive phase). The blast wave duration t_d can be determined by the following relation derived from the scaling law:

$$\frac{t_d}{W^{1/3}} = \frac{980\left[1+\left(\frac{Z}{0.54}\right)^{10}\right]}{\left[1+\left(\frac{Z}{0.02}\right)^3\right]\left[1+\left(\frac{Z}{0.74}\right)^6\right]\sqrt{1+\left(\frac{Z}{6.9}\right)^2}}. \tag{2}$$

2. SIMULATION OF EXPLOSION IN THE MSC.DYTRAN ENVIRONMENT

MSC.Dytran is a commercial software package for short-term transient analyses that involve structural as well as computational fluid dynamics facilities. The structures are modeled using a Lagrangian mesh, while a Eulerian[2] domain is used for the ambient air. The computational fluid dynamics solver of MSC.Dytran uses a Eulerian approach and employs a finite volume method to discretize the governing equations [9]. The use of the finite volume method ensures that the transported fluid-dynamic quantities are fully conserved, regardless of the mesh density.

The equations of the conservation laws are integrated in time by a first-order explicit dynamic procedure. The explicit approach accelerates computations because only the mass (diagonal) matrix has to be inverted. On the other hand, explicit techniques have the drawback of requiring very small time increments to provide accurate and stable solutions. Short-duration problems, such as explosion problems are usually solved by explicit methods convenient to solve problems involving very significant nonlinearities, which require continuous updating of stiffness matrices.

In simulations with fluid–structure interaction, the fluid inside a finite-volume domain is bounded by a coupling surface, which enables the fluid to exert a force on the deformable structure. A critical aspect of any Eulerian–Lagrangian fluid–shell coupling strategy is formulation of a theoretically sound and, at the same time, computationally effective algorithm that couples the fluid and shell solvers. For the explicit dynamics case, one approach involves coupling of two solvers by applying appropriate interface boundary conditions at the beginning of each time step. The interface boundary conditions follow from explicitly enforcing the continuity of normal velocity and the continuity of pressure at the interface. In the fluid solver, normal velocity continuity and free-tangential-flow (slip) boundary conditions are required for the inviscid Euler model. That may be enforced through a narrow band of cells outside the physical fluid domain. The field variables in these cells (the fluid velocity, pressure, and density) are chosen according to the solution within the physical domain and the shell velocity.

A number of different basic strategies have been proposed for coupling the response of interacting solids and fluids [10]. In the conventional arbitrary Lagrangian–Eulerian (ALE) approach, the coupling of

[2]The Euler mesh is stationary in space, while the fluid can flow through the mesh. The computational fluid method provides fluid velocity, pressure fields, and other variables.

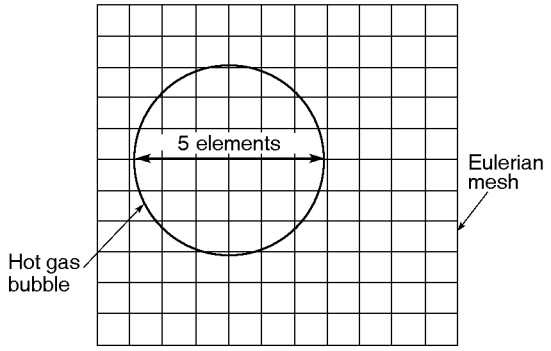

Fig. 2. Elements inside the bubble.

the fixed Eulerian and moving Lagrangian meshes is accomplished through an intermediate region in which the conforming mesh moves with a prescribed velocity. Details of mesh evolution in the intermediate region are critical for successful application of the ALE method, which, unfortunately, requires *a priori* information on the solution. Alternatively, a general coupling is used to simulate the interaction between the Lagrangian mesh and the Eulerian mesh. Multiple Eulerian domains are automatically generated around the coupling surface, and each Eulerian domain automatically adapts itself when the coupling surface moves and deforms. When the structures fail, the Eulerian materials flow through the holes in failed surfaces. This adaptive Eulerian domain technology can effectively simulate explosion phenomena by means of the MSC.Dytran software.

The MSC.Dytran software is based on the approximation of an instantaneous explosion. A hot gas bubble with high internal energy and pressure is formed in a quiescent environment. For this reason, to model the fluid inside and outside of the gas bubble, two subdomains are used. The outer domain surrounding the bubble containing the explosion products and consisting of air represents the environment where the structures are located, the external surfaces of aeronautic structures being subjected to boundary conditions of the domain (the blast wave propagates through this domain). The domain inside the bubble is filled by hot detonation products. Propagation of the blast wave is accompanied by mass, energy, and momentum flows, until the wave reaches the Lagrangian domain.

To model gas-bubble expansion, one has to determine the bubble size, density of explosion products, and their internal energy. The first parameter depends on the size of mesh elements. The accuracy increases with the sphere radius being reduced. Nevertheless, at least five elements must be used to have a good discretization of the bubble shape (Fig. 2). The specific energy and density can be written as:

$$E_b = E_{\mathrm{TNT}} = \frac{pV}{k-1}\left[1 - \left(\frac{p_a}{p}\right)^{(k-1)/k}\right], \qquad (3)$$

where

$$p = \rho_b RT\left(\frac{2}{5}\frac{e_b}{R}\right), \qquad (4)$$

E_b is the bubble energy, E_{TNT} is the real energy of the explosion in the TNT equivalent, ρ_b is the internal bubble density, e_b is the internal bubble energy, and R is universal gas constant. The analysis implied that $e_b = 7$ MJ/kg, which coincides with a trustworthy value of internal energy for this kind of simulations. Such an high value of energy is due to an explosion of a charge equivalent to 16 kg of TNT put into the bubble, which yields very high temperatures. The following initial values were used for the hot gas inside the bubble: $T = 9688$ K and $p = 7.56$ MPa; $p/p_a = 74.61$ at the sea level and $p/p_a = 197.64$ for $h = 7500$. The values obtained are listed in Table 1.

3. PRELIMINARY ANALYSIS

3.1. Simulation of an Explosion in Air

A preliminary analysis of an explosion of a powerful HE in free air was performed. Numerical results for the blast wave were compared with analytical formulations in Eqs. (1) and (2). A Eulerian mesh for standard air at the sea level (the air density is 1.225 kg/m^3) was generated. The following initial conditions were used: specific internal energy $e_a = 208$ kJ/kg, air pressure $p_a = 101$ kPa, radius of the bubble of explosion products 1.1 m, specific internal energy $e_b = 7$ MJ/kg, and HE mass 16 kg (the hot gas density is therefore, 2.87 kg/m^3). The duration of the blast wave was analytically estimated as $t_f = 0.02$ sec. Figure 3 shows the blast wave propagation. The peak pressures at five different nodes of the Eulerian domain are summarized in Table 2. The numerical and analytical results are compared in Fig. 4a. Only the first calculated point (the closest node to the explosion point) displays large discrepancies. Such an inconsistency is due to the gas-bubble size, which has been considered larger than the real case. For the remaining points, the results are in reasonable agreement with the analytical dependence.

Temperature calculations for air were performed in the same manner. Though high-pressure regions of the gas move faster than low-pressure regions, heat transfer is negligible because of the low thermal conductivity of air.

TABLE 1

Variation of the Charge Mass (TNT Equivalent) with the Bubble Size

r, m	V, m^3	E, MJ	m_{TNT}, kg	E, MJ	m_{TNT}, kg
		at sea level		at 7500 m altitude	
0.1	0.0042	0.056	0.012	0.062	0.013
0.2	0.034	0.45	0.096	0.49	0.11
0.3	0.11	1.5	0.32	1.7	0.36
0.4	0.27	3.6	0.77	3.9	0.84
0.5	0.52	7.0	1.5	7.7	1.6
0.6	0.9	12	2.6	13	2.8
0.7	1.44	19	4.1	21	4.5
0.8	2.15	29	6.1	32	6.7
0.9	3.05	41	8.7	45	9.6
1.0	4.2	56	12	62	13
1.1	5.6	75	16	82	17
1.2	7.2	97	21	107	23
1.3	9.2	123	26	136	29
1.4	11.5	154	33	169	36
1.5	14.1	189	40	208	44
1.6	17.2	230	49	253	54
1.7	20.6	276	59	303	65
1.8	24.4	327	70	360	77
1.9	28.7	385	82	423	90
2.0	33.5	449	96	493	105

The duration time is a very significant parameter for evaluating the blast wave damage effect. This parameter depends on the scale distance [see Eq. (2)]. The analytical and numerical values of t_d are compared in Fig. 4b, which shows good agreement between these results.

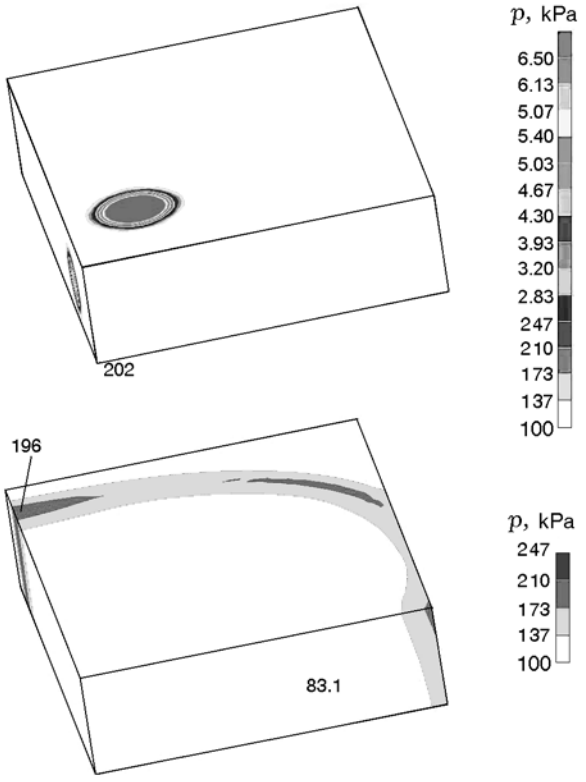

Fig. 3. Blast wave propagation model.

TABLE 2

Comparison of Analytical and Numerical Predictions of Peak Pressures

d, m	Z, m/kg$^{1/3}$	p^0, kPa	p^0/p_a	p^0, kPa	p^0/p_a
		formula (1)		numerical calculation	
3.78	1.50	405	4.0	1036	9.2
4.23	1.68	312	3.1	508	4.0
5.05	2.01	206	2.0	350	2.5
5.88	2.34	145	1.4	264	1.6
8.11	3.22	70	0.7	200	1

3.2. Effect of an Explosion on Simple Structures

In this paragraph, the explosion effects on panels and wing boxes are analyzed. First, the explosion effects on a stiff panel was considered. A $2 \times 2 \times 0.003$ m panel was immersed in the Eulerian mesh in the domain filled by air, so that the distance from an arbitrary element to the nearest boundary was at least 0.25 m. The size of the "Eulerian box" representing air was $4 \times 2.5 \times 2.5$ m. The panel was modeled with Lagrangian SHELL elements incorporating both the plasticity model and the failure model. Sixteen stiffeners shaped as omega bars were included. The panel and bars were modeled using aluminum 7075-T6 (usually used in aeronautic structures). Shell elements were used for the panel, while stiffeners were introduced as beam elements. Moreover, dummy elements were introduced behind the plate to generate a closed volume. An HE charge equivalent to 16 kg of TNT mass was placed at a distance of 2.7 m from the panel. The duration of the blast wave was assumed to be 0.01 sec.

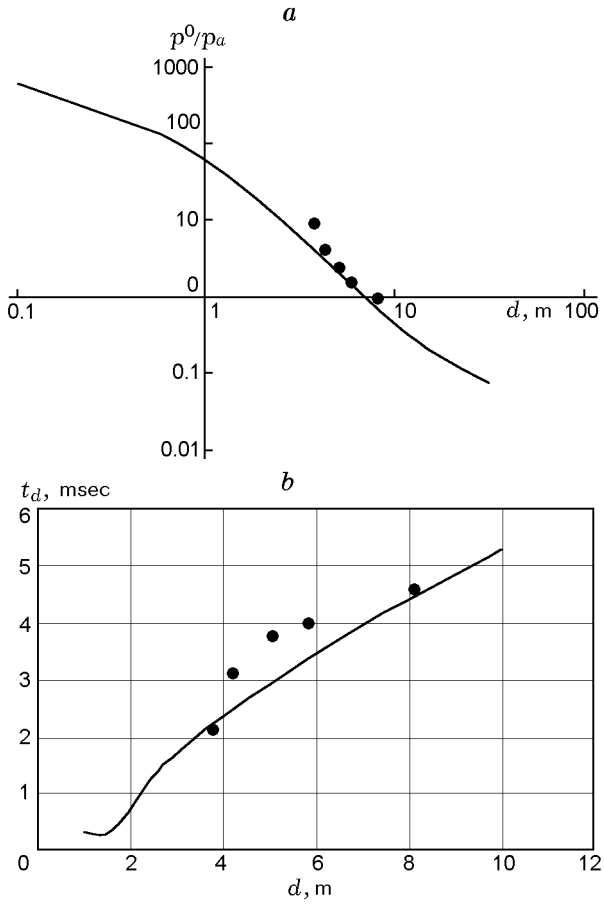

Fig. 4. Comparison between analytical (points) and numerical (curves) peak pressures (a) and duration (b) of the blast wave.

Panel damages caused by this explosion were observed. There were no failures, but the structure was seriously plastically deformed. Initially the plate bent outward under pressure loads, and then, after the blast wave passed, a depressive phase pulled the aluminum sheet backwards. By that moment, however, the panel had already reached plastic strain, so it was irreversibly deformed (Table 3). Figure 5 shows the time history of plastic strain at three different nodes. Curve 1 represents the central node. The deformation is assumed to start when the blast wave reaches the plate ($t \approx 1.5$ msec). Initially only elastic strain occurs, and then the yield stress was reached at a plastic strain of 0.48 GPa. By that moment, a bilinear behavior was defined to characterize the properties of the failing material. According to this model, the plastic stress is developed according to the follows relation:

$$\sigma_p = \sigma_0 + \frac{EE_h}{E - E_h}\,\varepsilon_p. \tag{5}$$

TABLE 3

Stiff Plate Behavior
Under the Action of a Blast Wave

TNT, kg	$\Delta l_{\max}$, m	$t_{\max}$, msec	$\sigma_{\max}$, MPa	ε, %	η, %
10	0.188	4.76	499	1.54	0
16	0.218	4.52	511	3.14	0
20	0.238	4.26	519	4.25	0
25	0.258	4.26	524	5.75	1.17
30	0.279	4.26	532	7.3	4.68
60	Failure	Failure	574	8*	91.4

Notes. $\Delta l_{\max}$ is the maximum displacement, $t_{\max}$ is the time when the maximum displacement is reached, $\sigma_{\max}$ is the maximum stress, ε is the strain, and η is the degree of failure; the values marked by the asterisk refer to the test where the failure occurs.

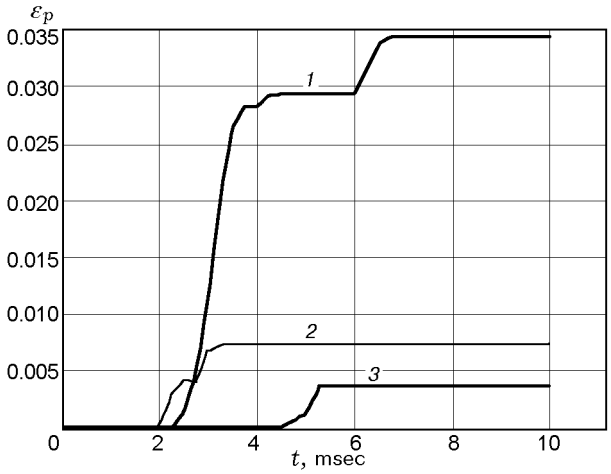

Fig. 5. Plastic history at the central node (curve 1), constrained edge (curve 2), and free edge (curve 3).

Here E is Young' modulus, E_h is the tangent of the plastic approximation straight line, σ_0 is the yield stress, σ_p is the plastic stress, and ε_p is the plastic strain. Then, we have

$$E_h = \frac{E\left(\dfrac{\sigma_r - \sigma_0}{\varepsilon_r}\right)}{E + \left(\dfrac{\sigma_r - \sigma_0}{\varepsilon_r}\right)}, \tag{6}$$

where σ_r and ε_r are the stress and strain values at the fracture point.

Further calculations were performed for a plate without stiffeners. In this case, the plate was rapidly and largely deformed by blast wave pressure loads, and failure occurred (see Fig. 6). A stiff plate was tested with seven different amounts of the HE. For an equiva-

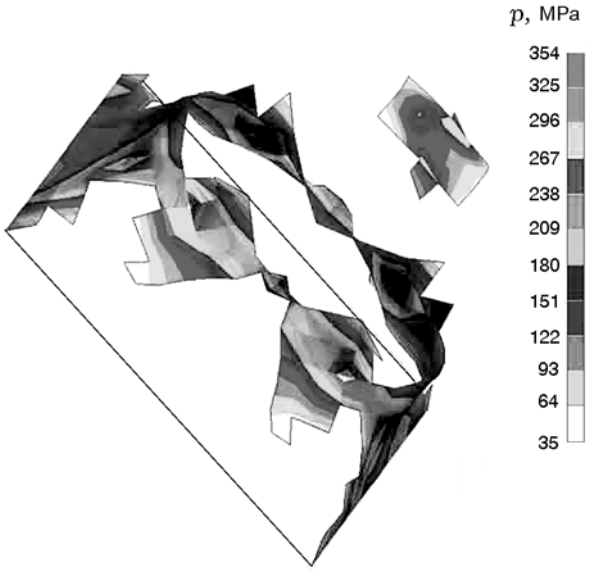

Fig. 6. Effect of an explosion of an HE equivalent to 16 kg TNT mass on the plate.

lent TNT mass between 10 and 60 kg, the central node displacement X_c was found to follow the linear law:

$$X_c = 0.0045W + 0.1446. \tag{7}$$

The most deformed regions were those at the plate corners. The failure percentage was set in the last corners. This parameter was the ratio of the number of failed mesh elements to the total number of plate elements.

3.3. Wing Box

The Catia geometric data for a wing box were imported into MSC.Dytran, in which an environment of finite-element meshes was made. The upper skin was made of the 7075-T6 aluminum alloy, while the bottom panels were made of the 2024-T3 aluminum alloy. All skin panels were assumed to be 5 mm thick. Eleven ribs and two spars were used as stiffeners inside the wing box. The explosion was simulated at an altitude of 7500 m from the sea level. Different variants with different locations of the HE charge explosion and equivalent TNT masses were considered. In the first calculation, an HE charge of 16-kg equivalent TNT mass was detonated in air, 1 m above the wing box and at a distance of 3 m from the leading edge. After 2.8 msec, the blast wave came in touch with the structure. The upper and lower skin panels are pressed inward with subsequent compression of stiffeners. This phenomenon involves large shear stress for the skin and buckling in the ribs. No damages on the wing box, however, were caused

Fig. 7. Effect of an explosion of an HE equivalent to 16-kg TNT mass on the wing box.

by this explosion. Plasticity occurs only in small regions. The effective stresses are plotted in Fig. 7. The explosion-point location was changed four times, but no significant differences were observed. It can be concluded that an explosion of 16 kg of equivalent TNT mass does not really damage the wing structure.

Different conclusions were obtained with 40 kg of equivalent TNT mass, located closer to the wing box at a distance of 1.7 m from the leading edge. In this case, the wing box underwent rapid plastic deformation, and fractures started in the skin. Obviously, the damage status depends on the explosion point location. A further case was investigated in which the explosive was put at a distance of 3 m from the leading edge. In this case, there were no evident fractures, but anyway plastic deformations were observed along all wing elements, and some tip ribs were broken.

One can conclude that a typical aeronautic aluminum panel could be destroyed if subjected to a blast wave explosion. Certainly, stiffeners improve the situation, but an HE charge of 40 kg of equivalent TNT mass could destroy the panel considered.

4. FULL AIRCRAFT SIMULATION

The benchmarks considered in the previous section demonstrated the possibilities of MSC.Dytran to simulate explosion phenomena. Such results encouraged us to develop a model for the analysis of an explosion on a flying aircraft. The explosion scenario in an aircraft in flight is extremely complex; the results can be affected by many complicating effects [11]. Two important facts should be considered in the explosion scenario:

• Evaluation of loads on the aircraft and their effects with allowance for flexibility of the aircraft structural elements;

• Evaluated of damage (plasticity, fracture, etc.) of aircraft structural elements.

Both of these issues play a critical role in developing a vulnerability study. Owing to available computational resources, however, attention was restricted to the first point. Therefore, an elastic mechanical model of the aircraft was considered. First, the pressure–load map was computed; it was further used for a comprehensive analysis. Some difficulties arise because of two different time scales inherent in the phenomenon: blast wave propagating with a high velocity and a comparatively slow elastic response of the aircraft structure as a whole (due to the large inertia).

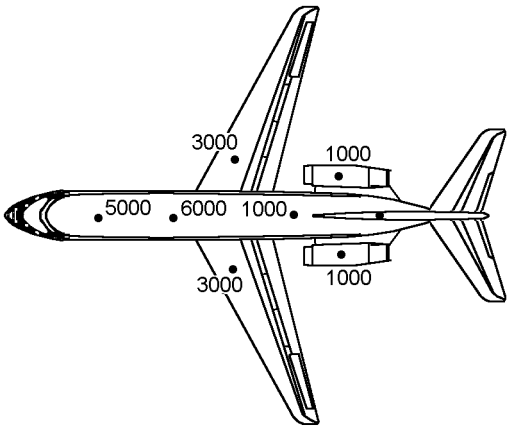

Fig. 8. Distribution of concentrated masses on the aircraft model (the values of equivalent masses are given in kilograms).

4.1. Description of the Finite-Element Model of the Aircraft

The external shape of the selected aircraft was very closed to a McDonnell–Douglas's DC9-30. A brief description of the simplified aircraft structure is provided in this section. The aircraft was assumed to accommodate 90 passengers and to have the maximum speed of 917 km/h. The propulsion system is constituted by two Pratt & Whitney JT8D-5 engines. The wings have a delta configuration with a 90 m^2 area. Their bending stiffness is due to two T-spars, 36 ribs, and 18 stringers. A typical cross-section of the fuselage can be basically constructed by two arcs. The passenger floor in the middle divides the cross-section into two parts: the upper portion for passengers and the lower one for cargo. A typical material for fuselage skins is 2024-T3 clad aluminum. The outer skin is reinforced by stringers aligned in the axial direction and by circumferential frames. Typical stringers and circumferential frames (omega sections) are made of 7075-T6 aluminum.

Numerical calculations were conducted by placing the HE charge near the plane. The MSC.Dytran model was used to investigate the immediate response of the structures to the explosion. The aircraft structures were immersed into the Eulerian mesh domain ($37 \times 27 \times 11$ m at 7500 m with standard air properties), so that distance from the explosion point was 5 m to the fuselage was 5 m and 3 m to the leading edge. The aircraft finite-element model employs two types of elements available in MSC.Dytran: bar and plate elements. Bar (BAR) elements were used for wing stiffeners, while most of the aircraft structures were modeled with shell elements, such as squares (QUAD4) and triangles (TRIA3). Hexagonal (HEXA) solid elements were used for the Eulerian mesh domain. In conclusion, the finite element model consisted of about 100,000 elements: 76,032 HEXA, 20,624 QUAD4, 1282 TRIA3, and 472 BAR elements. This model was employed to analyze the global effects of the blast wave on the aircraft, such as the overall stress and strain distributions and deformation patterns.

The MSC.Dytran model was build to study the fluid–structure interactions due to an external explosion next to the aircraft. To determine the pressure distribution over the aircraft external skin, particular care was taken on the generation of external geometry. The model consists of a quite good representation of the original geometry of the aircraft, but it is extremely conservative with regard to its stiffness. Moreover, a fictitious density was assigned at the shell, so that the model mass was equal to the mass of the empty aircraft. Finally, seven concentrated masses were put on the model to achieve the correct redistribution of the mass of the structure (see Fig. 8). Thermal effects of the explosion were neglected due to the low thermal conductivity of air.

4.2. Analysis and Results

Some selected results are presented in this section. First, the pressure loads due to the explosion are treated. We assume that the radius of the gas bubble is 1.4 m and its density is 0.93 kg/m^3 to keep the equivalent mass of 16 kg of the explosive. The results obtained are coherent with the analytical theory. The sequence of images in Fig. 9 shows the blast wave propagation along the external surface of the aircraft. Initially, the bubble comes in touch with the right wing of the model and collapses on it, causing pressure thrust. Figure 9 shows the maximum pressure value on the leading edges

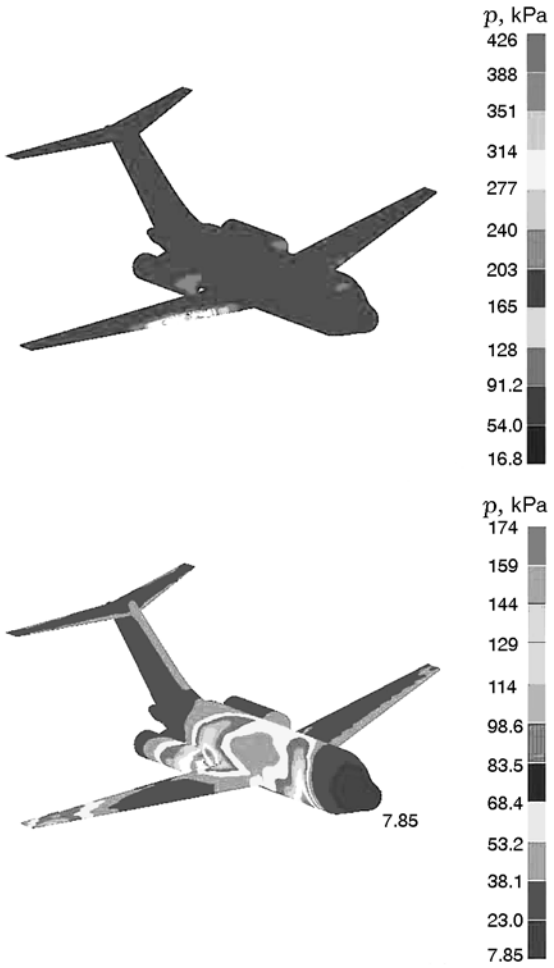

Fig. 9. Pressure fields of blast wave propagation on the external surface of the aircraft.

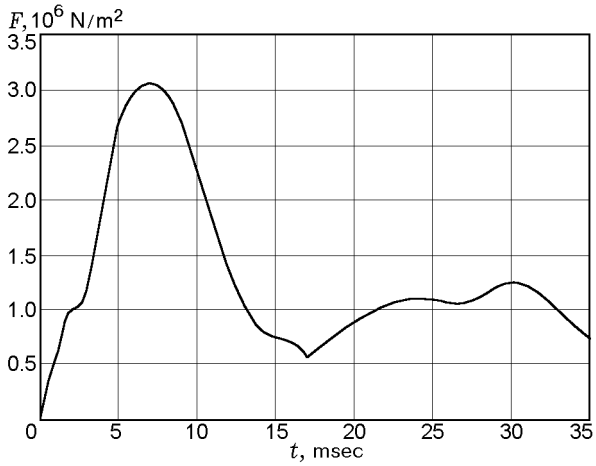

Fig. 10. Resultant component of pressure thrust.

of the wing (about 0.43 MPa). The calculations for panels proved that this value is sufficient for the plate to collapse. When the blast wave comes on the fuselage, the pressure value is lower than the one found on the leading edge (but the surfaces involved are wider). The panel analysis shows no damage on the structure. The only effect is a lateral force on the fuselage, which can be determined by integrating the pressure values on the fuselage surface. This value can be easily achieved using MSC.Dytran. The resultants of pressure thrust are plotted in Fig. 10. Thus, acceleration values along the three axes could be computed. Owing to a large aircraft inertia, it is not possible to see the aircraft elastic deformation at the explosion scale.

The attention was also focused on the analysis of the load factor n, which is a very important parameter to explore the vulnerability of commercial aircraft. The JAR 25 (Joint Aviation Requirements) writes that the maximum load factor for the aircraft considered is $n_{\max} = 3.75$. The diagrams in Fig. 10 show the load factors n along the three axis, by considering the following forces F_{x-z} and accelerations a_{x-z}:

$$\begin{aligned} &F_x = 980 \text{ kN}, && a_x = 21.77 \text{ m/sec}^2, && n_x = 2.21, \\ &F_y = -3000 \text{ kN}, && a_y = 66.66 \text{ m/sec}^2, && n_y = -6.79, \\ &F_z = 1500 \text{ kN}, && a_z = 33.33 \text{ m/sec}^2, && n_z = 3.40. \end{aligned}$$

It appears clear that the explosion considered could introduce loads that are not allowed by the structures. Moreover, small changes in the charge position could lead to inadmissible values of n_z.

Displacements generated by an explosion within the first few hundredths of a second are too small to be evaluated because of high inertia of the aircraft. At least 1-sec analysis should be considered to obtain appreciable displacements. A second analysis was, therefore, undertaken. The simulation was carried out for 1 sec. Because of a small step of integration in time required by explosion simulations, the CPU time required to run the model was about 700 h on a UNIX workstation computer. Figure 11 shows some configurations of the conducted analysis. More pictures, or better an animation, should be more appropriate to show the vibration induced by the explosion on the aircraft. Nevertheless, Fig. 11 clearly shows that the simulation can evaluate the effect of the explosion on a flying aircraft. The aircraft starts to vibrate; it moves in various directions. Simulations can predict the effect of the explosion position, HE amount, and aircraft speed on the loads acting on the aircraft and on the related vibration modes.

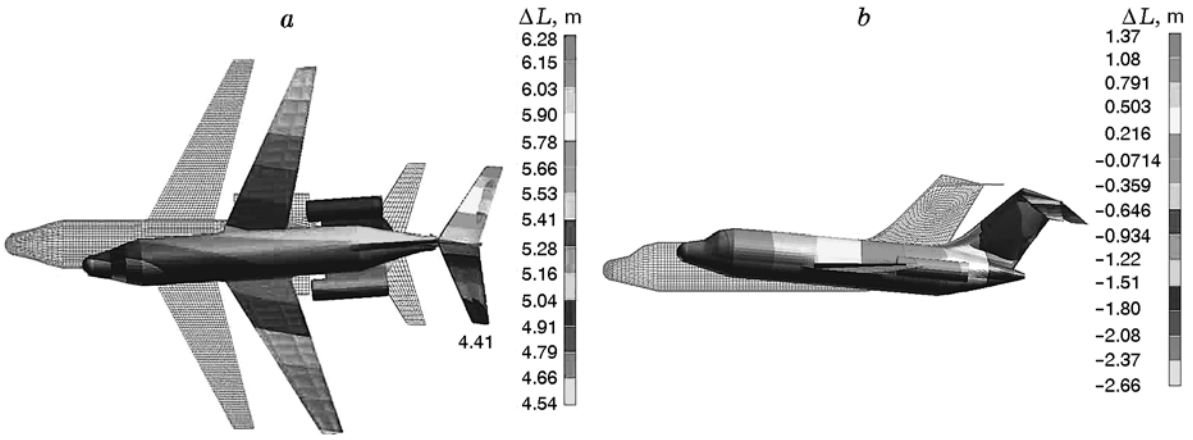

Fig. 11. Aircraft behavior after the explosion in the planes x–y (a) and x–z (b).

CONCLUSIONS

The study involved an analysis of the effect of an explosion on aeronautic structures. Rigid and deformable bodies were considered. The vibration caused on a full flexible aircraft was investigated. The studies showed the possibility of evaluating the loads on the aircraft for different initial positions of the explosion and different amounts of the HE charge. The modeling could permit a better design of the aircraft with respect to explosion phenomena and simulation of aircraft accidents, aimed at understanding their causes.

REFERENCES

1. A. L. Kuhl, J. C. Leyer, A. A. Borisov, and W. A. Sirignano (eds.), *Progress in Aeronautics and Astronautics*, Vol. 153: *Dynamic Aspects of Detonations*, AIAA (1993).
2. A. L. Kuhl, J. C. Leyer, A. A. Borisov, and W. A. Sirignano (eds.), *Progress in Aeronautics and Astronautics*, Vol. 154: *Dynamic Aspects of Explosion Phenomena*, AIAA (1993).
3. Abolhassan Astaneh-Asl, Casey Heydari, and Qiuhong Zhao, "Analysis of car-bomb effects on buildings using MSC-dytran software and protective measures," in: *Proc. of the MSC Software Virtual Product Development Conf.*, Dearborn, Michigan, October 13–15 (2003).
4. Jin Son, Abolhassan Astaneh-Asl, and Marcus Rutner, "Performance of bridge decks subjected to blast load," in: *6th Japanese–German Bridge-Symp.*, Munich, Germany (2005).
5. A. Morka, L. Kwasniewski, and J. W. Wekezer, "Assessment of passenger security in para-transit buses," *J. Public Transport*, **8**, No. 4 (2005).
6. D. Coppe, *Manuale Pratico di Esplosivistica Civile*, PEI Editore (1999).
7. MSC.Dytran User's Guide, MSC.Software (2004).
8. G. F. Kinney and K. J. Graham, *Explosive Shocks in Air*, Springer-Verlag (1985).
9. R. Eymard, Th. Gallouet, and R. Herbin, "Finite volume method," in: P. G. Ciarlet and J. L. Lions (eds.), *Handbook of Numerical Analysis*, Vol. 7, January (2003).
10. F. Cirak and R. Radovitzky, *A Lagrangian–Eulerian Shell-Fluid Coupling Algorithm Based on Level Sets*, Elseiver (2004).
11. Y. I. Moon, G. Bharatram, C. S. A. Schimmels, and D. V. B. Venkayya, "A vulnerability map of a commercial aircraft," Report, Structures Division, WL/FIBAD.